Crystal Structure of *fac*−Ir(ppy)$_3$ and Emission Properties under Ambient Conditions and at High Pressure†

Josef Breu,*,‡ Philipp Stössel,§ Sigurd Schrader,|| Alexander Starukhin,⊥ Walter J. Finkenzeller,# and Hartmut Yersin*,#

Lehrstuhl für Anorganische Chemie I, Universität Bayreuth, Universitätsstr. 30, D-95440 Bayreuth, Germany, Research and Development, Covion Organic Semiconducturs GmbH, D-65926 Frankfurt, Germany, Institute of Physics, Department of Condensed Matter Physics, University of Potsdam, Am Neuen Palais 10, D-14469 Potsdam, Germany, Institute of Molecular and Atomic Physics, National Academy of Sciences, 220072 Minsk, Belarus, and Institut für Physikalische Chemie, Universität Regensburg, D-93040 Regensburg, Germany

Received August 11, 2004. Revised Manuscript Received November 19, 2004

Solution and refinement of the crystal structure of *fac*−Ir(ppy)$_3$ is severely hampered by systematic twinning and pseudo-symmetry. *fac*−Ir(ppy)$_3$ crystallizes in the centrosymmetric space group $P\bar{3}$ as has been deduced from single-crystal structure refinement and investigations of the second harmonic generation (SHG) of *fac*−Ir(ppy)$_3$ powder as compared to two standard materials. The topology of the molecular packing of *fac*−Ir(ppy)$_3$ is identical to the packing observed for [Ru(bpy)$_3$]^0, however, the site symmetry of all Ir(ppy)$_3$ molecules is necessarily lowered from D_3 to C_3. Packing motifs with intermolecular "$\pi-\pi$ interactions" of T-shaped and "shifted π stack" geometry are realized. The systematic twinning leads to the occurrence of crystalline domains with rigorously alternating chirality within the bulk of the domains but with homochiral *fac*-Ir(ppy)$_3$ contacts at the domain interfaces. These differences in packing motifs are displayed in the emission spectra and in the high-pressure-induced shifts of the emission. The emission maximum of the bulk material at 18 350 cm^{-1} (545 nm) and of the domain interfaces at 19 700 cm^{-1} (507 nm) experience for $p < 25$ kbar and $T = 295$ K red shifts of $\Delta\bar{\nu}/\Delta p = -(12 \pm 2)$ cm^{-1}/kbar, and $-(22 \pm 4)$ cm^{-1}/kbar, respectively.

1. Introduction

The tris-chelated orthometalated *fac*−Ir(ppy)$_3$ complex (with ppy = 2-phenyl pyridine anion) has been known for nearly two decades.[1,2] Recently, it became particularly attractive due to its very high efficiency of electrophosphorescence in organometallic light-emitting devices (OLEDs).[3−5] The high efficiency of this material is based on the specific trapping mechanisms of injected electrons and holes, on the high quantum yield of the triplet → singlet phosphorescence of about 40% at ambient temperature,[2] and on the high intersystem crossing efficiency from the excited singlet to the triplet. Thus, the excitation energy is harvested in the lowest excited triplet which is responsible for light emission of the OLED.[3−6] The high electroluminescence yield of triplet emitters is essentially governed by spin−orbit coupling (soc) carried by the d-orbitals of the transition metal ion. Therefore, purely organic OLED materials with weak soc effects will not exhibit comparably high electro-luminescence yields.

Due to the importance of *fac*−Ir(ppy)$_3$ for green light-emitting OLEDs it is of interest to study the electronic structure of this compound in more detail. From low-temperature spectroscopic investigations[7−11] and theoretical studies[12] of the ground state and lower lying excited states, though without inclusion of spin−orbit coupling, the assignment of the emitting triplet as metal-to-ligand charge transfer (^{3}MLCT) is now possible. However, highly resolved optical spectra, as have been recorded and interpreted for other organo−transition metal compounds, such as Pt(thpy)$_2$ or Pt(thpy)(CO)(Cl)[13,14] with thpy = 2-(2-thienyl)-pyridinate

† Dedicated to Professor Rüdiger Kniep on the occasion of his 60th birthday.

* Authors to whom correspondence should be addressed. H.Y.: fax, +49 941/9434488; e-mail, hartmut.yersin@chemie.uni-regensburg.de. J.B.: fax, +49 921 552788; e-mail, josef.breu@uni-bayreuth.de.

‡ Universität Bayreuth.

§ Covion Organic Semiconducturs GmbH.

|| University of Potsdam. Present address: University of Applied Sciences Wildau.

⊥ National Academy of Sciences.

Universität Regensburg.

(1) Dedeian, K.; Djurovich, P. I.; Garces, F. O.; Carlson, G.; Watts, R. J.; *Inorg. Chem.* **1991**, *30*, 1685−1687.
(2) King, K. A.; Spellane, P. J.; Watts, R. J. *J. Am. Chem. Soc.* **1985**, *107*, 1431−1433. Stoessel, P.; Spreitzer, H.; Becker, H. Covion Organic Semiconductors. WO 02/060910, 2001.
(3) Lamansky, S.; Djurovich, P.; Murphy, D.; Abdel-Razzaq, F.; Kwong, R.; Tsyba, I.; Bortz, M.; Mui, B.; Bau, R.; Thompson, M. E. *Inorg. Chem.* **2001**, *40*, 1704−1711.
(4) Yang, X. H.; Neher, D. *Appl. Phys. Lett.* **2004**, *84*, 2476−2478.
(5) Laskar, I. R.; Chen, T.-M. *Chem. Mater.* **2004**, *16*, 111−117.
(6) Yersin, H. *Top. Curr. Chem.* **2004**, *241*, 1−26.
(7) Colombo, M. G.; Brunold, T. C.; Riedener, T.; Güdel, H. U. *Inorg. Chem.* **1994**, *33*, 545−550.
(8) Colombo, M. G.; Hauser, A.; Güdel, H. U. *Top. Curr. Chem.* **1994**, *171*, 143−171.
(9) Finkenzeller, W. J.; Yersin, H.; *Chem. Phys. Lett.* **2003**, *377*, 299−305.
(10) Finkenzeller, W. J.; Stössel, P.; Yersin, H. *Chem. Phys. Lett.* **2004**, *397*, 289−295.
(11) Finkenzeller, W. J.; Stössel, P.; Kulikova, M.; Yersin, H. *Proc. SPIE* **2004**, *5214*, 356−367.
(12) Hay, P. J. *J. Phys. Chem. A* **2002**, *106*, 1634−1641.
(13) Yersin, H.; Donges, D.; Humbs, W.; Strasser, J.; Sitters, R.; Glasbeek, M. *Inorg. Chem.* **2002**, *41*, 4915−4922.
(14) Yersin, H.; Donges, D. *Top. Curr. Chem.* **2001**, *214*, 81−186.

10.1021/cm0486767 CCC: $30.25
Published on Web 03/08/2005

could not be measured yet. Nevertheless, it will be shown below that even the spectrally broad emission displays characteristic features of the crystal structure.

Additionally, the crystal structure of *fac*−$Ir(ppy)_3$ is attractive with respect to more fundamental studies in crystal engineering. Each crystal structure contains a wealth of valuable information about how the multitude of noncovalent intermolecular interactions compete and collaborate to achieve their subtle balance.[15] Careful analysis of crystal structures and packing motifs will release the inherent information and will assist in developing a better understanding of the "grammar of crystal packing".[16]

Tris-chelated metal complexes of planar bis-dendate ligands, such as $[M(L-L)_3]^{n+}$ (e.g., L−L: ppy, phen = 1,10-phenanthroline or bpy = 2,2′-bipyridine) are especially well suited to study crystal packing systematics.[17−20] On one hand, these propeller-shaped, chiral molecules display a very corrugated molecular shape. In Lehn's[21] notation, there is a lot of information stored at the molecular level which inevitably will be read out at the supramolecular level when neighboring molecules penetrate each other to achieve maximum packing density. On the other hand, this molecular recognition will not be obscured by massive intramolecular changes since the molecules are rather rigid. Being a neutral compound, with *fac*−$Ir(ppy)_3$, intermolecular interactions may be analyzed without the interference of strong ionic interactions between anions and cations and without the additional spatial requirements imposed by the anions.

2. Experimental and Background

Synthesis. *fac*−$Ir(ppy)_3$ was prepared according to a modified procedure first reported by Watts et al.[2] The product was purified by recrystallization from DMSO and/or acetonitrile in an inert atmosphere until a purity of >99.9% (HPLC) was achieved. In particular, ^1H NMR investigations show that the concentration of *mer*-$Ir(ppy)_3$ is less than 0.1%. Single crystals suitable for X-ray diffraction were obtained by slow evaporation from DMSO and/or acetonitrile at an elevated temperature (T = 50 °C).

Emission Spectra. The emission spectra under ambient conditions were recorded by use of a Fluorolog 3 (Jobin Yvon) and/or equipment as described in ref 22. High-pressure measurements were carried out with a diamond anvil cell similar to the one described in ref 22. Pressure calibration was performed by use of the red shift of the R_1-line of small ruby crystals placed near to the *fac*−$Ir(ppy)_3$ crystal within the high-pressure chamber. The R_1 line is shifted by $\Delta\bar{\nu}/\Delta p = -0.75$ cm^{-1}/kbar[23] (1 kbar = 10^8 Pa). The total amount of red shift under applied pressure was determined relative to the energy position of a plasma line of a low-pressure discharge lamp placed outside the high-pressure cell. The sample itself and the ruby crystal, respectively, were excited by an Ar ion laser line of λ_{exc} = 363.8 nm.

Table 1. Crystallographic Data and Details of the Structure Determination; *fac*−$Ir(ppy)_3$ Crystallizes in Space Group $P\bar{3}$ (No. 147)

		fac−$[Ir(ppy)_3]$	
formula		$C_{33}H_{24}IrN_3$	
formula weight		654.75	
crystal system		trigonal	
a [Å]		16.8003(10)	
c [Å]		15.3998(10)	
V [Å^3]		3764.3(4)	
Z		6	
D_x [g/cm^3]		1.733	
F(000)		1920	
μ [cm^{-1}]		5.348	
crystal size [mm]		0.1 × 0.1 × 0.5	
crystal shape		hexagonal needle	
crystal color		yellow	
temperature [K]		173(2)	
radiation [Å]		Mo Kα 0.71069	
θ range [deg]		2.65−26.36	
h		−20/20	
k		−20/20	
l		−19/19	
total no. of reflections		29547	
space group		$P\bar{3}c1$ (No. 165) (incorrect supergroup)	$P\bar{3}$ (No. 147)
orientation of dipole moments in	$^1/_3$, $^2/_3$, ∼0	↑	↑
	$^2/_3$, $^1/_3$, ∼0	↓	↓
	0, 0, ∼0.25	↕	↑↓
restraints applied[a]	DELU	yes	yes
	SAME	no	yes
	DEFIX	no	yes
	ISOR	N51	
uniq. reflections		2568	4854
R_{int}		0.0568	0.0552
observed refl. [$I_o > 2\sigma(I_o)$]		1603	2744
refined parameters		171	339
R1[b]		0.0336	0.0334
wR2(all)[c]		0.0799	0.0674
S (restraint, all)[d]		1.051	1.079
d, e[e]		0.0455, 0.0	0.0295, 0.0
BASF		0.66267	0.66302
$\Delta\rho_{min}$, $\Delta\rho_{max}$·[e$^-$/Å^3]		−0.929, 2.275	−0.850, 2.279

[a] For atom labeling, see Supporting Informationn. [b] $R1 = \sum||F_o| - |F_c||/\sum|F_o|$. [c] $wR2 = \{\sum[w(F_o^2 - F_c^2)^2]/\sum[w(F_o^2)^2]\}^{1/2}$. [d] $S = \{\sum[w(F_o^2 - F_c^2)^2]/(n-p)\}^{1/2}$ with n = no. of refl. and p = total no. of parameters refined. [e] $w = 1/[\sigma^2(F_o^2) + (dP)^2 + eP]$ with $P = [2F_c^2 + \mathrm{Max}(F_o^2,0)]/3$.

Crystal Structure Analysis. Relevant crystallographic data and details of the data collection and structure refinement are listed in Table 1.

The data are affected by systematic twinning by merohedry (twin law: 0 −1 0, −1 0 0, 0 0 −1). This lamellar twinning is already indicated by the gritty appearance of crystal faces. The twinning renders structure solution with Patterson or direct methods impossible. Instead, initial coordinates for the refinement were taken from the related structures of $[M(bpy)_3]^0$ (M = Ti, V, Cr, Ru).[24,25] The apparent Laue-symmetry of the twin is $P(6/m)mm$.[26] As early as 1963 Albrecht[24] realized that with Z = 6, as deduced from the cell volume, it is impossible to accomplish this high symmetry with molecules of point group symmetry D_3 and lower. For the $[M(bpy)_3]^0$ complexes (M = Ti, V, Cr) Albrecht suggested the correct space group $P\bar{3}c1$ of the merohedric twin. With the very

(15) Aakeröy, C. B. *Acta Crystallogr. B* **1997**, *53*, 569−586.
(16) Brock, C. P.; Dunitz, J. D. *Chem. Mater.* **1994**, *6*, 1118−1127.
(17) Rillema, D. P.; Jones, D. S.; Woods, C.; Levy, H. A. *Inorg. Chem.* **1992**, *31*, 2935−2938.
(18) Breu, J.; Domel, H.; Stoll, A. J. *Eur. J. Inorg. Chem.* **2000**, 2401−2408.
(19) Breu, J.; Seidl, W.; Huttner, D.; Kraus, F. *Chem.—Eur. J.* **2002**, *8*, 4454−4460.
(20) Breu, J.; Stoll, A. J. *Acta Crystallogr. C* **1996**, *52*, 1174−1177.
(21) Lehn, J. M. *Pure Appl. Chem.* **1994**, *66*, 1961−1966.
(22) Stock, M.; Yersin, H. *Chem. Phys. Lett.* **1976**, *40*, 423−429.
(23) Forman, R. A.; Piermarini, G. J.; Barnett, J. D.; Block, S. *Rev. Sci. Instrum.* **1972**, *176*, 284.
(24) Albrecht, G. *Z. Chem.* **1963**, *3*, 182−187.
(25) Perez-Cordero, E.; Campana, C.; Echegoyen, L. *Angew. Chem.* **1997**, *109*, 85−88; *Angew. Chem., Int. Ed. Engl.* **1997**, *36*, 137−140.
(26) Araki, T. *Z. Kristallogr.* **1991**, *194*, 161−191.

limited means available at that time (optical analogy methods) he even was able to partially solve the structure of the twin. Only the *z*−coordinates of the molecule at the Wyckhoff position 2a were wrong. The complete structure solution was published in 1997 by Echegoyen et al.[25] for the isomorphic $[Ru(bpy)_3]^0$.

After introducing the above-mentioned twin law, it is formally possible to refine the structure of *fac*−Ir(ppy)$_3$ in the same space group $P\bar{3}c1$ found for $[M(bpy)_3]^0$. However, this implies the site symmetry D_3 for the occupied Wyckhoff position 2a at 0, 0, *z*. In contrast to this, the maximum site symmetry for *fac*−Ir(ppy)$_3$ is only C_3, and the molecule possesses a dipole moment. Therefore, at this formal site the pyridine and phenyl parts of the ligands are artificially connected by symmetry and an average Ir−N and Ir−C bond length of 2.065(7) Å results. Consequently, when refining in this incorrect supergroup ($P\bar{3}c1$) it was necessary to restrain the atomic displacement parameter (ADP) for one N by using a restraint (ISOR) to prevent it from going non-positive definite. Also, the *wR2* is comparatively high (Table 1).

Thus, the symmetry has to be lowered into one of the subgroups of $P\bar{3}c1$ that releases the symmetry of this 2a-site to C_3 or lower. The choices are the centrosymmetric space group $P\bar{3}$ or the polar space group *P*3*c*1. In *P*3*c*1, again three possibilities exist with respect to the orientation of the dipole moments within the three columns in the unit cell. Keeping in mind that the observed diffraction pattern of the merohedric twin shows a high pseudo symmetry of *P*(6/*m*)*mm*, it is obvious that it will be impossible to distinguish between these alternatives solely on the basis of structure refinement. However, $P\bar{3}$ and *P*3*c*1 may be conclusively distinguished by an investigation of effects of second harmonic generation (SHG). Since no significant SHG could be measured (Section 3.2), the centrosymmetric space group $P\bar{3}$ appears to be the right choice. Even though the space group cannot be deduced decisively from the diffraction data, the details of the refinement, in line with the SHG experiment (see Section 3.2), favor the centrosymmetric structure. (1) When refining in the incorrect noncentrosymmetric space group *P*3*c*1, the Flack parameter[27] suggests ($x \approx 0.5$) that besides general twinning, additionally racemic twinning has to be refined simultaneously. (2) Also, while refinement in the incorrect polar space group leads to *wR2* values of comparable magnitude, many additional restraints are required for stable and physically sensible refinements as compared to refinement in $P\bar{3}$.

For reasons of completeness, it should be mentioned that the possibility of solvent inclusion was checked utilizing PLATON's "CALC SOLVENT" feature. No residual solvent-accessible voids could be identified.

The final structure refinement as listed in Table 1 was therefore carried out in $P\bar{3}$ applying the SHELX-97 program package.[28,29] SHELX refines against F^2 and all data were used in the full-matrix least-squares. H atoms were placed in idealized positions and refined with fixed isotropic displacement parameters of $1.2U_{eq}$ (parent C). All other atoms were refined anisotropically. The weighting scheme recommended by the program was used and refinement was continued until complete convergence (maximum shift/esd < 0.001) was achieved. Graphics and geometrical parameters were prepared using the PLATON package.[30]

Crystallographic data (excluding structure factors) for the $P\bar{3}$ refined structure reported in this paper have been deposited with the Cambridge Crystallographic Data Centre as supplementary publication CCDC-245671. Copies of the data can be obtained free of charge on application to CCDC, 12 Union Road, Cambridge CB2 1EZ, UK [Fax int. code +44(1223)336-033; E-mail deposit@ccdc.cam.ac.uk].

Second Harmonic Generation. Second harmonic generation (SHG) requires noncentrosymmetric structures both of the molecule involved and of its packing in ordered structures. Therefore, SHG can help to decide whether the investigated crystal structure is centrosymmetric or not. The molecule *fac*−Ir(ppy)$_3$ is noncentrosymmetric. Its ground-state dipole moment has been calculated[31] to 6.5 D. Moreover, the lowest excited states are based on charge-transfer transitions with nonvanishing changes of the dipole moment, therefore a nonvanishing second-order hyperpolarizability β can be expected.[32] This is confirmed by ab initio quantum chemical calculations which provide a second-order hyperpolarizability of at least two times higher than that of para-nitroaniline.[33] Hence, if *fac*−Ir(ppy)$_3$ would crystallize in a noncentrosymmetric space group, then a significant second-order response of the bulk material should occur.

For SHG measurements crystalline particles (average size $\approx$ 6 μm) were placed between two glass slides (refractive index n = 1.51) in a way that the particles were positioned close to each other without overlap. Thus, an area of a few cm^2 was covered with isolated particles. The thickness of this layer was assumed to be that of the average particle size. As light source for SHG measurements an active-passive mode locked Nd:YAG laser (BM Industries, France) was used. It emits laser pulses of 21 ps duration at a wavelength of 1064 nm and an energy of 8 mJ per pulse with a repetition rate of 10 Hz. The diameter of the laser spot at the sample plane was 1 mm. The pulse energy was reduced to 1 mJ per pulse by use of filters. SHG measurements have been carried out in transmission. In front of the sample, all second harmonic (SH) light generated by various optical components was blocked by a filter. After transmission through the sample, the light was collected and focused by a lens on the entrance slit of a monochromator. The detection wavelength for the second harmonic (SH) was tuned with a spectral resolution of 0.1 nm over a narrow spectral range around 532 nm. The fundamental wave behind the sample was blocked by an appropriate filter before the beam entered the monochromator. A photomultiplier was used for detection of the SH light.

For comparison, powder samples of para-nitroaniline (PNA) and 2-methyl-4-nitroaniline (MNA) also have been measured under the same conditions. The SH signal of the MNA sample was extremely high and therefore attenuated by means of a gray filter with a transmission coefficient of 0.005 at 532 nm in order to stay in the linear range of the photomultiplier. For PNA and *fac*−Ir(ppy)$_3$, the SH light was detected without a gray filter.

The average size of PNA and MNA crystals was about (10 $\pm$ 1) μm. Thus, in both cases, the average crystal size was slightly larger than that of the *fac*−Ir(ppy)$_3$ samples. The average coverage of the investigated area with particles was 25% for all three compounds.

PNA and MNA are noncentrosymmetric molecules, both having dipole moments of 6.2 D.[34] The average second-order hyperpolarizability β of PNA and MNA are $\beta = 9.2 \times 10^{-30}$ esu and $\beta = 8.7 \times 10^{-30}$ esu, respectively. These values were measured by means of electric field-induced second harmonic generation (EFISH)

(27) Flack, H. D. *Acta Crystallogr. A* **1983**, *39*, 876−881.
(28) Herbst-Irmer, R.; Sheldrick, G. M. *Acta Crystallogr. B* **1998**, *54*, 443−449.
(29) Sheldrick, G. M. *SHELX-97*. University of Göttingen, 1997.
(30) Spek, A. L. *Acta Crystallogr. A* **1990**, *46*, C34.
(31) Hay, P. J., private communication.
(32) Prasad, P. N.; Williams, D. J. *Introduction to Nonlinear Optical Effects in Molecules and Polymers*; John Wiley and Sons: New York, 1991.
(33) Agren, H.; private communication.
(34) Singer, K. D.; Hubbard, S. F.; Schober, A.; Hayden, L. M.; Johnson, K. Second Harmonic Generation. In Kuzyk, M. G.; Dirk, C. W. *Characterization Techniques and Tabulations for Organic Nonlinear Optical Materials*; Marcel Dekker: New York, 1998; pp 311−513.

at 1064 nm in solution.[34] PNA forms centrosymmetric crystals. Thus, all nonlinear optical effects of even order are vanishing. Therefore, no SHG signal is expected from PNA bulk material. Only at the crystal surface and interfaces, for which a break of symmetry is present, a significant SHG signal is generated. On the other hand, MNA crystals are noncentrosymmetric.[35] They are among the first organic single crystals studied with respect to their second-order nonlinear optical properties.[36] The crystal structure of MNA is monoclinic and thus, according to Zyss and Oudar,[37] belongs to the most successful point groups for frequency doubling.[32]

The comparison of the SHG response of powder samples of crystalline *fac*−Ir(ppy)$_3$ with the response of the two other materials should allow us to decide whether *fac*−Ir(ppy)$_3$ crystallizes in a centrosymmetric or a noncentrosymmetric structure.

3. Results and Discussion

3.1. Crystal Structure. *3.1.1. Topology of Molecular Packing.* Due to the rigid planar structure of the ppy-ligands, *fac*−Ir(ppy)$_3$ is far from being spherical; it possesses three major "pockets" between two ligands and additionally two minor "pockets" along the 3-fold molecular axis. In a closed packed crystal structure, extensive mutual penetration of neighboring molecules is required. The packing patterns observed indicate preferred intermolecular interactions.

The topology of the molecular packing of *fac*−Ir(ppy)$_3$ is identical to the packing observed[25] for $[Ru(bpy)_3]^0$, which crystallizes in $P\bar{3}c1$ with one out of three symmetry independent complex molecules at a special site with D_3 point symmetry. However, since the maximum point symmetry of *fac*−Ir(ppy)$_3$ is C_3 this compound must crystallize in a space group of lower symmetry. The correct space group of *fac*−Ir(ppy)$_3$ indeed turns out to be $P\bar{3}$. The crystal structure of *fac*−Ir(ppy)$_3$ represents a true racemate. The unit cell contains a total of three Λ− and three Δ−complexes, which all occupy special sites with site symmetry C_3. The six molecules are arranged in three columns running along *c*. Λ− and Δ−molecules are stacked rigorously alternating in the columns (compare Figure 3a and Figure 4). The center of symmetry relates the Λ− and Δ−molecules within the column at 0, 0, *z* (Wyckhoff positions 2a), while for the columns at $^1/_3$, $^2/_3$, *z* and $^2/_3$, $^1/_3$, *z* (Wyckhoff positions 2b and 2c) the respective symmetry equivalent molecules are exchanged between the columns and shifted in *z* ($z = z + ^1/_2$). The orientation of the molecules is fixed by the site symmetry—the C_3 axis must be collinear with the *c* axis. The Ir−Ir distance within each column is 8.402 Å. The two columns at $^1/_3$, $^2/_3$, *z* and $^2/_3$, $^1/_3$, *z* are at the same "height" along c and make up two honeycomblike hexagonal layers in the *ab* plane at $z = 0$ and $z = ^1/_2$, respectively (Figure 1). Within the layers, neighboring molecules at the same "height" have opposite chirality. For instance, the Λ−complex at $^1/_3$, $^2/_3$, 0 is surrounded by three Δ−complexes at $^2/_3$, $^1/_3$, 0; $-^1/_3$, $^1/_3$, 0; and $^2/_3$, $^4/_3$, 0. This motif of a racemic honeycomblike hexagonal layer is also found in the crystal

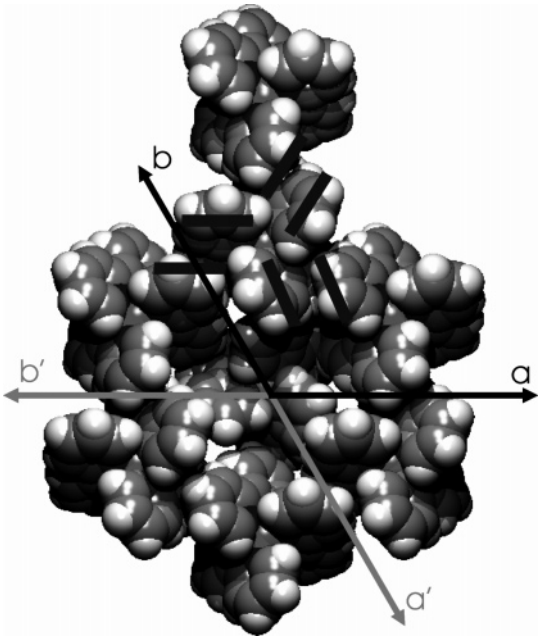

Figure 1. Space-filling packing diagram of molecular layers in *fac*−Ir(ppy)$_3$. Axes of both twin domains are shown. The "shifted−π−stack"-type interlocking of adjacent molecules at the 2b and 2c sites is indicated by parallel bars.

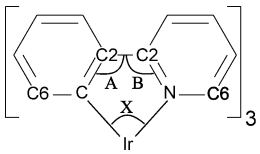

Figure 2. Labeling scheme of geometrical parameters listed in Table 2.

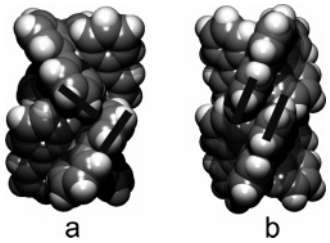

Figure 3. (a) Space-filling packing diagram of columns of complexes running along *c* in *fac*−Ir(ppy)$_3$. In the ideal structure, T-type "π−π−interactions" are realized along *c*. (b) However, systematic twinning leads to some "shifted−π−stack"-type interlocking of adjacent molecules at the twin boundary as also observed in $[Ni(bpdz)_3](ClO_4)_2$.[39]

structure of $[Ru(bpym)_3](PF_6)_2 \cdot CH_3CN$[17] (bpym = 2,2′-bipyrimidine). The motifs differ only in the size of the cavity in the center of the honeycomb. In $[Ru(bpym)_3](PF_6)_2 \cdot CH_3CN$ the Ru−Ru distance between neighboring complexes is comparatively short (8.047, 8.122, and 8.653 Å) and thus the cavity is small and it only fits a small acetonitrile as solvate molecule. The Ir−Ir distance between adjacent molecules in the hexagonal layers of *fac*−Ir(ppy)$_3$, however, is much longer (3×9.709 Å). The resulting cavity is therefore larger and it is filled by two Ir(ppy)$_3$ molecules, which belong to the third independent column located at 0, 0, *z* in the unit cell. This third column is displaced along *z* ($z = 0.2500$ and $z = 0.7500$) relative to the columns which make up the hexagonal layers. Consequently, two *fac*−Ir(ppy)$_3$ molecules intrude from above and below into the cavity of the hexagonal layer (Figure 1). The distances between the Ir metal centers in the layers and those lying in

(35) Lipscomb, G. F.; Garito, A. F.; Narang, R. S. *J. Chem. Phys.* **1981**, *75*, 1509−1516.
(36) Levine, B. F.; Bethea, C. G.; Thurmond, C. D.; Lynch, R. T.; Bernstein, J. L. *J. Appl. Phys.* **1979**, *50*, 2523−2527.
(37) Zyss, J.; Oudar, J. L. *Phys. Rev. A* **1982**, *26*, 2028−2048.

Table 2. Selected Intramolecular Parameters Observed for *fac*−Ir(ppy)$_3$ Compared to Theoretical and Average Values Deposited in the Cambridge Crystallographic Data Base (CCD)[38] [a]

[Å]/[deg]		Ir−C	Ir−N	N−C6	N−C2	C−C6	C−C2	A	B	X
DFT-optimized[12]		2.035	2.167							
CSD-mean ($N = 25$)		2.006(4)	2.088(9)	1.345(6)	1.358(4)	1.405(5)	1.423(5)	115.5(3)	114.0(3)	80.0(2)
	$^1/_3$, $^2/_3$, ∼0	2.034(9)	2.086(8)	1.379(11)	1.378(11)	1.415(11)	1.391(11)	113.7(7)	115.1(7)	78.6(4)
$P\bar{3}$	$^2/_3$, $^1/_3$, ∼0	2.032(9)	2.095(9)	1.382(11)	1.383(11)	1.403(11)	1.402(11)	114.2(7)	114.9(7)	79.0(4)
	0, 0, ∼0.25	2.060(10)	2.071(10)	1.361(12)	1.385(12)	1.374(12)	1.396(12)	115.7(8)	115.8(8)	79.6(4)

[a] For a labeling scheme see Figure 2.

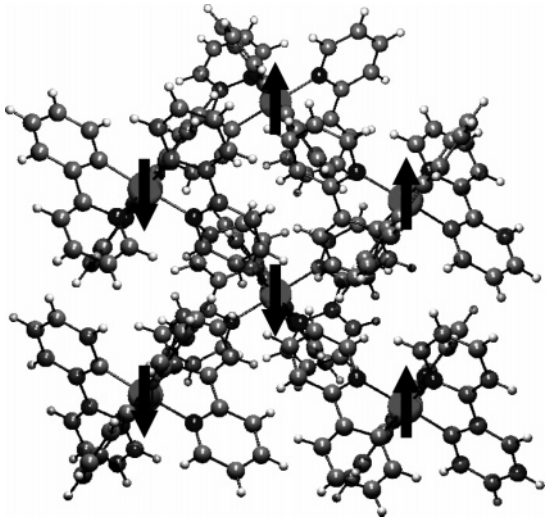

Figure 4. Crystal packing diagram of *fac*−Ir(ppy)$_3$. Orientation of the dipole moments in the three columns running along *c* at positions $^1/_3$, $^2/_3$, *z* (left), $^2/_3$, $^1/_3$, *z* (right), and 0, 0, *z* (middle). In this centrosymmetric space group $P\bar{3}$ a tail−tail arrangement of dipole moments occurs at 0, 0, *z*.

the cavities is comparatively long (Ir−Ir = 10.357−10.519 Å).

The molecular structure of all three independent molecules is in close agreement with both theoretical values and related structures of ppy complexes (Table 2) deposited in the Cambridge Crystallographic Data Base (CCD).[38] The asymmetry with short Ir−C and long Ir−N distances is correctly reproduced.

3.1.2. π−π−Interactions. The intermolecular interactions for both packing motifs (columns and layers) occurring in the structure appear to be controlled by so-called "π−π−interactions".[40−44] On one hand, along the racemic columns a T-shaped geometry of adjacent aromatic ligands is accomplished (Figure 3a). On the other hand, in the hexagonal layers each ligand of the central molecule is involved in a "shifted π−stack" with three adjacent molecules (Figure 1).

Lateral interactions of this kind are popular motifs in crystal packings of aromatic compounds[45,46] and their general importance in molecular recognition has been acknowledged.[47,48] Recent experimental[43,49,50] and theoretical[51−54] work has shown that both dispersion forces and electrostatic C−H···π−interactions contribute toward the favorable "π−π−interactions". The relative importance of these two contributions is a matter of debate,[49,50] especially for the T-shaped arrangement. The inherent polarity of aromatic systems stems from the electron-rich core being surrounded by an electron-poor torus of hydrogens. This electrostatic contribution accounts for the energetic preference of both T-shaped and shifted π−stacked arrangements. Which of these is the preferred one for a particular system depends on the relative magnitude of dispersion- and C−H···π−interactions and therefore on the planar extension of the aromatic system. Even for the simplest system, the benzene dimer in gas phase, there is an ongoing dispute which local minimum on the potential energy hypersurface represents the more stable configuration.[53−58] In the solid state of planar aromatic molecules the two local minima manifest themselves in herringbone and/or π−stacked crystal packing motifs.[45,46,59]

With $[M(L-L)_3]^{n+}$, the situation is more complicated than with simple aromatic systems since the fixation of three aromatic ligands in a rigid mutual orientation imposes certain spatial requirements that also involve the chirality of these complexes. For these concerted "π−π−interactions" even a special nomenclature has been introduced by Dance.[60,61] Despite the spatial restraints imposed by the coordination, "π−π−interactions" are frequently observed in crystal

(38) Allen, F. H.; Kennard, O. *Chem. Des. Autom. News* **1993**, *8*, 31−37.
(39) Onggo, D.; Rae, A. D.; Goodwin, H. A. *Inorg. Chim. Acta* **1990**, *178*, 151−163.
(40) Liljefors, T.; Petterssen, I. *J. Comput. Chem.* **1987**, *8*, 1139−1145.
(41) Jorgensen, W. L.; Severance, D. L. *J. Am. Chem. Soc.* **1990**, *112*, 4768−4774.
(42) Hunter, C. A. Non-Covalent Interactions Between Aromatic Molecules. In *From Simplicity to Complexity in Chemistry − and Beyond;* Vieweg: Braunschweig, 1996; pp 113−126.
(43) Hunter, C. A.; Lawson, K. R.; Perkins, J.; Urch, C. J. *J. Chem. Soc., Perkin Trans. 2* **2001**, 651−669.
(44) Carver, F. J.; Hunter, C. A.; Livingstone, D. J.; McCabe, J. F.; Seward, E. M. *Chem.—Eur. J.* **2002**, *8*, 2848−2859.
(45) Desiraju, G. R.; Gavezzotti, A. *Acta Crystallogr. B* **1989**, *45*, 473−482.
(46) Dunitz, J. D.; Gavezzotti, A. *Acc. Chem. Res.* **1999**, *32*, 677−684.
(47) Hunter, C. A. *Angew. Chem., Int. Ed. Engl.* **1993**, *32*, 1584−1586.
(48) Adams, H.; Harris, K. D. M.; Hembury, G. A.; Hunter, C. A.; Livingstone, D.; McCabe, J. F. *J. Chem. Soc. Chem. Commun.* **1996**, 2531−2532.
(49) Wilcox, C. S.; Kim, E.; Paliwal, S. *J. Am. Chem. Soc.* **1998**, *120*, 11192−11193.
(50) Wilcox, C. S.; Paliwal, S.; Geib, S. *J. Am. Chem. Soc.* **1994**, *116*, 4497−4498.
(51) Karlström, G.; Linse, P.; Wallqvist, A.; Jönsson, B. *J. Am. Chem. Soc.* **1983**, *105*, 3777−3782.
(52) Jorgensen, W. L.; Severance, D. L.; Duffy, E. M. Modeling interactions with benzene: Aryl−aryl, cation−π, and chaotrope−π. In *Computational Approaches in Supramolecular Chemistry*; Kluwer Academic Publishers: Dordrecht, 1994; pp 161−173.
(53) Hobza, P.; Selzle, H. L.; Schlag, E. W. *J. Phys. Chem.* **1996**, *100*, 18790−18794.
(54) Hobza, P.; Spirko, V.; Selzle, H. L.; Schlag, E. W. *J. Phys. Chem. A* **1998**, *102*, 2501−2504.
(55) Scherzer, W.; Kratzschmar, O.; Selzle, H. L.; Schlag, E. W. *Z. Naturforsch. (A)* **1992**, *47*, 1248−1252.
(56) Venturo, V. A.; Felker, P. M. *J. Chem. Phys.* **1993**, *99*, 748−751.
(57) Arunan, E.; Gutowsky, H. S. *J. Chem. Phys.* **1993**, *98*, 4294−4296.
(58) Niesse, J. A.; Mayne, H. R. *J. Phys. Chem.* **1997**, *101*, 9137.
(59) Gavezzotti, A. *Chem. Phys. Lett.* **1989**, *161*, 67−72.
(60) Russell, V.; Scudder, M.; Dance, I. *J. Chem. Soc., Dalton Trans.* **2001**, 789−799.
(61) Dance, I.; Scudder, M. *J. Chem. Soc., Dalton Trans.* **1998**, 1341−1350.

structures of propeller-shaped molecules of the type investigated here.[17,18,20,25,60−62]

However, it should be stressed that despite the ubiquity of "$\pi-\pi-$interactions" in *fac*−Ir(ppy)$_3$ nothing can be said about the relative importance of dispersion/repulsion forces and the electrostatic C−H···$\pi-$interactions contributing to these "$\pi-\pi-$interactions".

Kuroda et al.[63,64] calculated the dispersion energies for active (enantiomerically pure) and racemic pairs of propeller-shaped, chiral [M(L−L)$_3$]^0 molecules with D_3 symmetry. As a model compound a tris(butadienyl)metal complex has been used and the dispersion energy was calculated using an extended transition monopole model. For a racemic pair two energy minima were identified. The global minimum was observed with parallel C_3 axes similar to the situation realized in the hexagonal layers of *fac*−Ir(ppy)$_3$. The second, local minimum was found with collinear C_3 axes, the arrangement that is found along the columns in *fac*−Ir(ppy)$_3$. In other words, the observed T-shaped and "shifted $\pi-$stack" arrangements do not only optimize the electrostatic C−H···$\pi-$interactions but also the dispersion forces, because the mutual orientations of adjacent molecules allow an efficient packing. It cannot be decided which of the two, C−H···π or dispersion, is the pivotal driving force for the observed intermolecular packing patterns. Rather, both interactions seem to be of similar importance.

This statement is also supported by the occurrence of systematic twinning. The general twin law (0 −1 0, −1 0 0, 0 0 −1) interchanges the symmetry related molecules at the Wyckoff position 2a in $z = 0.2500$ and $z = 0.7500$ and disrupts the rigorous alternation of $\Lambda-$ and $\Delta-$molecules along *c*. At the twin boundary an active pair with collinear C_3 axes is created (Figure 3b). For such an active pair adjacent ligands are no longer engaged in a T-shaped geometry but rather in a shifted $\pi-$stack involving half of a ligand. The systematic nature of this twinning suggests that active and racemic contacts with collinear C_3 axes are close in energy. And indeed, this was already predicted by Kuroda et al.[63,64] They found an active pair with collinear arrangement of C_3 axes to have an even shorter contact separation than the racemic pair, although the dispersion energy is slightly smaller than that for the racemic pair.

The approximate energetic equivalence of these two intermolecular contacts is further underlined by the crystal structure of [Ni(bpdz)$_3$](ClO$_4$)$_2$[39] (bpdz = 3,3′-bibpyridazine). [Ni(bpdz)$_3$](ClO$_4$)$_2$ crystallizes in a Sohncke space group (*P*321) and the structure consists of homochiral columns of complex cations with collinear C_3 axes (as shown in Figure 3b). Interestingly, this structure is also twinned producing the opposite transition from a homochiral to a racemic contact at the twin boundary.

3.1.3. Dipole−Dipole-Interactions. While the topology of the molecular packing of *fac*−Ir(ppy)$_3$ is identical to the one of [Ru(bpy)$_3$]^{0}[25] the site symmetry of the molecules must be lower due to the lower symmetry of the ppy-ligand. The pyridine moieties of all three ligands are arranged in a *facial* fashion. They point into the same direction along the C_3 axis and the molecule possesses a significant dipole moment. Thus, the maximum site symmetry in agreement with the molecular structure is only C_3. It should be noted that although C and N have similar diffraction power, without twinning problems it could conclusively be distinguished between the phenyl and the pyridine side of the ligand (Table 2). This is because Ir−C and Ir−N distances differ by almost 0.1 Å. Consequently, the molecular geometry of the whole ligand is distorted and the deviations from D_3 are considerable.

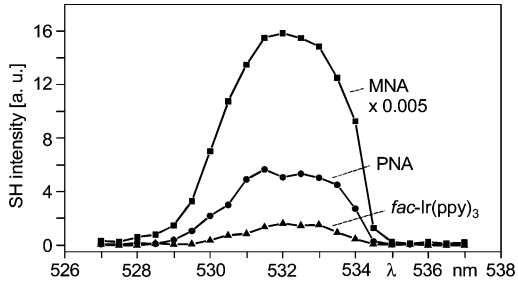

Figure 5. SHG intensity of powder samples of *fac*−Ir(ppy)$_3$ compared to 2-methyl-4-nitroaniline (MNA, attenuated) and para-nitroaniline (PNA) at 300 K, fundamental 1064 nm.

For *fac*−Ir(ppy)$_3$, a quite large dipole moment of 6.5 D has been calculated.[31] The dipole moments in the columns that make up the honeycomblike hexagonal cavities are oriented as expected: (1) within the columns the dipole moments are aligned head to tail; (2) if the dipole moment in the column at $^1/_3$, $^2/_3$, 0 is pointing in the $-c$ direction, the dipole moments of the three neighboring columns at $^2/_3$, $^1/_3$, 0; $-^1/_3$, $^1/_3$, 0; and $^2/_3$, $^4/_3$, 0 are pointing in the $+c$ direction. However, the dipole moments of the molecules in the column at 0, 0, *z* are aligned tail to tail, which is energetically unfavorable (Figure 4). At the twin boundaries, the tail−tail arrangement is converted into a more advantageous head−tail one. This will additionally foster systematic twinning.

3.2. Comparison of SHG Intensities of *fac*-Ir(ppy)$_3$, PNA, and MNA. Figure 5 compares the SHG intensity plots of powder samples of 2-methyl-4-nitroaniline (MNA, SH intensity reduced by a factor of 0.005), para-nitroaniline (PNA), and *fac*−Ir(ppy)$_3$ with average powder coverage of ∼25% in each case. These results clearly show that the detected SHG signal of *fac*−Ir(ppy)$_3$ powder is very weak, in particular, when compared with the SH intensity found for the noncentrosymmetric MNA. Its SH intensity is more than 3 orders of magnitude higher than the one of *fac*−Ir(ppy)$_3$. This is due to the noncentrosymmetric space group of MNA crystals which allows SHG from the bulk material. On the other hand PNA, although a noncentrosymmetric molecule, crystallizes centrosymmetrically. Therefore, the bulk signal of PNA is zero. The SH signal which is still detectable results from crystal surfaces with an inherent symmetry break. For *fac*−Ir(ppy)$_3$ powder, showing even a significantly smaller SH response than the PNA powder, the SH intensity is similarly ascribed to the crystal surfaces and additionally to twin boundaries. The average particle size

(62) Janiak, C. *J. Chem. Soc., Dalton Trans.* **2000**, 3885−3896.
(63) Kuroda, R.; Mason, S. F.; Rodger, C. D.; Seal, R. H. *Mol. Phys.* **1981**, *42*, 33−50.
(64) Kuroda, R.; Biscarini, P. *Mol. Cryst. Liq. Cryst. Sci. Technol. A.* **1996**, *278*, 275−284.

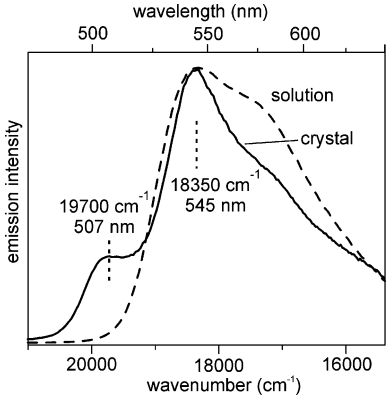

Figure 6. Comparison of emission spectra of a single-crystal of *fac*-Ir(ppy)$_3$ (λ_{exc} = 320 nm) to Ir(ppy)$_3$ dissolved in acetonitrile (10^{-4} mol/L; λ_{exc} = 300 nm) at T = 300 K. The emission maximum of the dissolved compound lies at 19 420 cm^{-1} (515 nm). For a better comparison, this spectrum is shifted by 30 nm to the red. The two spectra are normalized to their maxima.

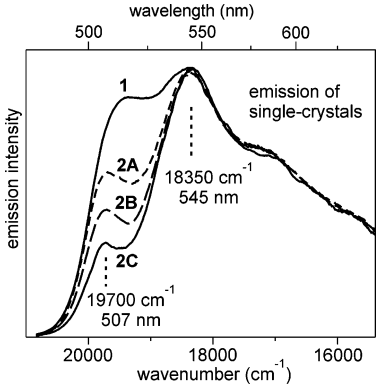

Figure 7. Emission spectra of two *fac*-Ir(ppy)$_3$ single-crystals 1 and 2. The spectra 2A, 2B, and 2C are measured at different positions of the same crystal surface of crystal 2, T = 300 K, λ_{exc} = 363.8 nm. All spectra are normalized to the maximum at 18 350 cm^{-1}.

of the *fac*−Ir(ppy)$_3$ sample was only slightly smaller than those of the PNA or MNA samples, but this difference of only 20% cannot explain the large differences between the SH intensities of the three materials. In conclusion, the results clearly show that *fac*−Ir(ppy)$_3$ crystallizes in a centrosymmetric space group. (Compare the background presented in Section 2.)

3.3. Photoluminescence at Ambient Conditions and Under High Pressure. *fac*−Ir(ppy)$_3$ is a green triplet emitter and plays a prominent role in the rapidly developing field of OLED technology. Therefore, a detailed study of emission properties of isolated complexes, but also of the crystalline material, is of high interest. Moreover, an investigation of the emission behavior can reveal valuable information about structural properties and irregularities of the crystalline material. In this respect, the situation is not favorable for *fac*−Ir(ppy)$_3$, since it has not yet been possible to obtain well-resolved and thus sufficiently informative optical spectra, even though isolated (dissolved) *fac*−Ir(ppy)$_3$ complexes have been investigated by methods of site-selective spectroscopy at low temperature down to T = 1.2 K.

Nevertheless, from the temperature and magnetic field dependence of the broad emission spectra and the temperature development of the emission decay time it was possible to determine the energy level diagram and the individual emission decay times of the three lowest excited and emitting states, **I**, **II**, and **III**.[9−11] In particular, the energy separations from the lowest excited state **I** are $\Delta E_{II,I}$ = 13.5 cm^{-1} and $\Delta E_{III,I}$ = 83 cm^{-1}. For the emission decay times one finds τ_I = 145 μs, τ_{II} = 11 μs, and τ_{III} = 750 ns. These states have been assigned to substates of a ^{3}**MLCT** term of mainly Ir5d-ppyπ* character. It follows that the emission properties at ambient temperature are determined by at least these three states. The resulting average decay time is 2.1 μs.[9] Experimentally, one finds a decay time of τ(300 K) = 1.9 μs in degassed acetonitrile.[1]

The emission spectrum of crystalline *fac*−Ir(ppy)$_3$ exhibits an interesting deviation from the spectrum of the dissolved compound. The crystals investigated were of good optical quality, as visually inspected under a microscope. Figure 6 compares the two spectra recorded at 300 K. The spectrum of *fac*−Ir(ppy)$_3$ dissolved in acetonitrile at a concentration of about 10^{-4} mol/L has its emission maximum at 19420 cm^{-1} (515 nm). It is reproduced in Figure 6 after having been shifted by 1070 cm^{-1} (30 nm) to lower energy to allow a better comparison. The amount of such an energy shift due to a variation of the immediate environment is not unusual.

The emission spectrum of *fac*−Ir(ppy)$_3$ single crystals is characterized by the occurrence of a shoulder at 19 700 cm^{-1} (507 nm) at the high energy side of the main maximum at 18 350 cm^{-1} (545 nm). Interestingly, a corresponding high energy shoulder is not present in the spectrum of the dissolved compound. Thus, an assignment of this shoulder to a higher lying intrinsic electronic state of the *fac*−Ir(ppy)$_3$ complex is improbable. This is further substantiated by the results summarized in Figure 7, where emission spectra of two different single crystals **1** and **2** are compared. Moreover, the spectra of crystal **2** are recorded at three different positions of the same crystal surface **2A**, **2B**, and **2C**. The spectra in Figure 7 are normalized to the emission maximum at 545 nm (18350 cm^{-1}). It is clearly shown that the emission intensity of the high-energy shoulder varies strongly from crystal to crystal, but also with the specific position of a given crystal. It is of further importance that the excitation spectrum as well as the rise of the absorption spectrum fit to the emission of the main peak having its maximum at 18 350 cm^{-1}. Thus, it is strongly indicated that the corresponding low-energy peak has to be assigned to the majority of emitting molecules (bulk material).

The behavior described can be related to irregularities of the crystal structure due the systematic twinning (Section 3.1). The systematic twinning with many thin (lamellar) domains stacked along *c* generates many homochiral contacts at the twin boundaries. Although the bulk material in the different domains will have an identical electronic structure (since adjacent domains are related by the twin law), distinct distortions occur at the domain interfaces. In particular, with the active pair generated at twin boundaries adjacent ligands are no longer engaged in a T-shaped geometry but rather in a shifted π−stack involving half of a ligand. Moreover, this homochiral contact created at the twin boundary may be slightly shorter than the 8.402 Å observed in the bulk of the material (see discussion in Section 3.1.2). Obviously, this distortion will result in distinct electronic energy shifts of

those complexes that lie directly at the interfaces, but also of the second, third, etc. nearest neighbors.

These distorted complexes seem to be responsible for the emission observed as a high energy shoulder in the spectra of the crystalline material. Specifically, the smaller the size of the domains, the larger is the number of interfaces (per volume). Thus, a reduction of domain size causes an increase of the emission intensity of the high energy shoulder. From the model presented it follows that the domain size strongly varies from crystal to crystal and also with the specific position investigated of a given crystal.

Obviously, crystalline *fac*−Ir(ppy)$_3$ with its intrinsic disorder is not well suited for high-resolution spectroscopy. The distortions experienced by the *fac*−Ir(ppy)$_3$ complexes are distinctly inhomogeneous. Consequently, the spectral inhomogeneity is large and hence the spectra are broad. Thus, even at low temperature (1.2 K), it was not possible to obtain well-resolved spectra.[9] Examples with a more suitable behavior are given in refs 65 and 66

For completeness, it is remarked that the nonsymmetry related complexes of the unit cell of a regular domain (bulk material) will also have different electronic transition energies. However, the corresponding emission would not depend on the spatial position within one specific single crystal. Therefore, this alternative interpretation does not apply to the experimental situation.

Investigations of emission spectra under variation of high pressure can provide additional insight into the electronic structure and the significance of specific intermolecular interactions.[67−69] Therefore, we studied the emission of single crystals of *fac*−Ir(ppy)$_3$ up to about 80 kbar. The measurements were carried out at ambient temperature by use of a diamond anvil cell. We investigated a crystal which exhibits an emission spectrum such as spectrum **1** of Figure 7. This spectrum shows two distinct emission maxima. Under application of high pressure, the high energy peak at 19 700 cm^{-1} (507 nm shoulder) is shifted by $-(22 \pm 4)$ cm^{-1}/kbar, while the main maximum at 18 350 cm^{-1} (545 nm) experiences a smaller shift of $\Delta\bar{\nu}/\Delta p = -(12 \pm 2)$ cm^{-1}/kbar. Within limits of experimental error, both pressure-induced shifts are linear up to about 25 kbar (for higher pressure, see below.).

Generally, a pressure-induced shift of an electronic transition is induced by the combined effects of an inherent intramolecular compression and a change of interactions of the chromophore with its environment. Both effects can be of similar importance. This is strongly indicated by high pressure studies of compounds in different environments.[70,71] The pressure-induced red shift of the main emission maximum at 18 350 cm^{-1}, assigned to the bulk of the domains, with $\Delta\bar{\nu}/\Delta p = -(12 \pm 2)$ cm^{-1}/kbar (for $p < 25$ kbar) compares well with the shift found for single crystals of [Ru(bpy)$_3$](PF$_6$)$_2$ with $\Delta\bar{\nu}/\Delta p = -(9 \pm 2)$ cm^{-1}/kbar (electronic origin at 17 816 cm^{-1}, $T = 1.7$ K[72]). This result is not unexpected, since the emitting states of both compounds stem from ^{3}**MLCT** states[9,73] and the intermolecular interactions are of similar character. For both compounds they are largely controlled by alternating Λ− and Δ−contacts along the *c*-axes.[65]

Interestingly, the pressure-induced shift of the high-energy emission maximum at 19 700 cm^{-1} is nearly twice as large as the shift of the low energy peak. In the scope of the assignment of the high-energy peak to molecules near the twin boundaries, a distinctly different $\Delta\bar{\nu}/\Delta p$ value is expected. At the interfaces, the Λ/Δ−alternation of *fac*−Ir(ppy)$_3$ is lifted. The resulting homochiral Λ/Λ− and Δ/Δ− contacts, respectively, will experience a significantly modified change of the intermolecular interactions induced by high-pressure application.

For completeness it is mentioned that for $p > 25$ kbar the emission structure disappears. This is a consequence of the decreasing energy separation of the two peaks and spectral broadening effects. Thus, only the shift of the overall emission maximum can be identified. For this maximum, one finds a much smaller value of about −2 cm^{-1}/kbar for $25 < p \leq 80$ kbar. Such a small value of pressure-induced shift is not unusual at high pressure. It can be related to a small compressibility at higher pressure (e.g., see refs 67 and 69).

Acknowledgment. We are grateful to the DFG, the Fonds der Chemischen Industrie, and the Bundesministerium für Bildung und Forschung (BMBF) for financial support. We thank Viachaslau Ksianzou (University of Potsdam) for his support in carrying out SHG measurements.

Supporting Information Available: Crystallographic information for *fac*−Ir(ppy)$_3$ (CIF). This material is available free of charge via the Internet at http://pubs.acs.org.

CM0486767

(65) Breu, J.; Kratzer, C.; Yersin, H. *J. Am. Chem. Soc.* **2000**, *122*, 2548−2555.
(66) Yersin, H.; Kratzer, C. *Coord. Chem. Rev.* **2002**, *229*, 75−93.
(67) Drickamer, H. G.; Frank, C. W. *Electronic Transitions and the High-Pressure Chemistry and Physics of Solids*; Chapman and Hall: London, 1973.
(68) Bray, K. L. *Top. Curr. Chem.* **2001**, *213*, 1−94.
(69) Yersin, H.; Hidvegi, I.; Gliemann, G.; Stock, M. *Phys. Rev. B.* **1979**, *19*, 177−180.
(70) Offen, H. W.; Hein, D. E. *J. Chem. Phys.* **1969**, *50*, 5274−5278.
(71) Yersin, H.; Trümbach, D.; Wiedenhofer, H. *Inorg. Chem.* **1999**, *38*, 1411−1415.
(72) Trümbach, D. Ph.D. Thesis, Regensburg, 1995.
(73) Yersin, H.; Humbs, W.; Strasser, J. *Top. Curr. Chem.* **1997**, *191*, 153−249.